Atmos. Chem. Phys. Discuss., 15, 15289–15317, 2015
www.atmos-chem-phys-discuss.net/15/15289/2015/
doi:10.5194/acpd-15-15289-2015

Atmospheric Chemistry and Physics
Discussions
Open Access

Neutral atmosphere temperature change at 90 km, 70° N, 19° E, 2003–2014

S. E. Holmen[1,2,3], C. M. Hall[2], and M. Tsutsumi[4,5]

[1]The University Centre in Svalbard, Longyearbyen, Norway
[2]Tromsø Geophysical Observatory, UiT – The Arctic University of Norway, Tromsø, Norway
[3]Birkeland Centre for Space Science, Bergen, Norway
[4]National Institute of Polar Research, Tokyo, Japan
[5]The Graduate University for Advanced Studies (SOKENDAI), Department of Polar Science, Hayama, Japan

Received: 28 April 2015 – Accepted: 12 May 2015 – Published: 5 June 2015

Correspondence to: S. E. Holmen (siljeh@unis.no)

Published by Copernicus Publications on behalf of the European Geosciences Union.

Abstract

Neutral temperatures for 90 km height above Tromsø, Norway, have been determined using ambipolar diffusion coefficients calculated from meteor echo fading times using the Nippon/Norway Tromsø Meteor Radar (NTMR). Daily temperature averages have been calculated from November 2003 to October 2014 and calibrated against temperature measurements from the Microwave Limb Sounder (MLS) on board Aura. The long-term trend of temperatures from the NTMR radar is investigated, and winter and summer seasons are looked at separately. Seasonal variation has been accounted for, as well as solar response, using the F10.7 cm flux as a proxy for solar activity. The long-term temperature trend from 2003 to 2014 is $-3.6\,\mathrm{K} \pm 1.1\,\mathrm{K\,decade^{-1}}$, with summer and winter trends $-0.8\,\mathrm{K} \pm 2.9\,\mathrm{K\,decade^{-1}}$ and $-8.1\,\mathrm{K} \pm 2.5\,\mathrm{K\,decade^{-1}}$, respectively. How well suited a meteor radar is for estimating neutral temperatures at 90 km using meteor trail echoes is discussed, and physical explanations behind a cooling trend are proposed.

1 Introduction

Temperature changes in the mesosphere and lower thermosphere (MLT) region due to both natural and anthropogenic variations cannot be assessed without understanding the dynamical, radiative and chemical couplings between the different atmospheric layers. Processes responsible for heating and cooling in the MLT region are many. Absorption of UV by O_3 and O_2 causes heating, while CO_2 causes strong radiative cooling. Planetary waves (PWs) and gravity waves (GWs) break and deposit heat and momentum into the middle atmosphere and influence the mesospheric residual circulation, which is the summer-to-winter circulation in the mesosphere. Also, heat is transported through advection and adiabatic processes.

For decades, it has been generally accepted that increased anthropogenic emissions of greenhouse gases are responsible for warming of the lower atmosphere (e.g.

Manabe and Wetherald, 1975), and that these emissions are causing the mesosphere and thermosphere to cool (Akmaev and Fomichev, 2000; Roble and Dickinson, 1989). Akmaev and Fomichev (1998) reported, using a middle atmospheric model, that if CO_2 concentrations are doubled, temperatures will decrease by about 14 K at the stratopause, by about 10 K in the upper mesosphere and by 40–50 K in the thermosphere. Newer and more sophisticated models include important radiative and dynamical processes as well as interactive chemistries, and they predict that the cooling rate near the mesopause is less than previously expected. The thermal response in this region is strongly influenced by changes in dynamics, and some dynamical processes contribute to a warming which counteracts the cooling expected from greenhouse gas emissions (Schmidt et al., 2006).

Even though the increasing concentration of greenhouse gases is generally accepted to be the main driver, also other drivers of long-term changes and temperature trends exist, namely stratospheric ozone depletion, long-term changes of solar and geomagnetic activity, secular changes of the Earth's magnetic field, long-term changes of atmospheric circulation and mesospheric water vapour concentration (Laštovička et al., 2012). The complexity of temperature trends in the MLT region and their causes act as motivation for studying these matters further.

In this paper, we investigate long-term trends of temperatures obtained from the NTMR radar, and we also look at summer and winter seasons separately. In Sect. 2, specifications of the NTMR radar are given, and the theory behind the retrieval of temperatures using ambipolar diffusion coefficients from meteor trail echoes is explained. In Sect. 3, the method behind the calibration of NTMR temperatures against Aura MLS temperatures is explained. Section 4 treats the temperature trend analysis, including the correction for seasonal variation and solar response. The theory and underlying assumptions for the method of determining neutral temperatures from meteor trail echoes and thus how well suited a meteor radar is for estimating such temperatures is discussed in Sect. 5. Also, physical explanations behind the trend are discussed, as well as comparison with other reports on trends.

ACPD
15, 15289–15317, 2015

2 Instrumentation and data

The Nippon/Tromsø Meteor Radar (NTMR) is located at Ramfjordmoen near Tromsø, at 69.58° N, 19.22° E. It is operated 24 h a day, all year round. Measurements are available for more than 90 % of all days since the radar was first operative in November 2003. The meteor radar consists of one transmitter antenna and five receivers and is operating at 30.25 MHz. It detects echoes from ionized trails from meteors, which appear when meteors enter and interact with the Earth's neutral atmosphere in the MLT region. The ionized atoms from the meteors are thermalized, and the resulting trails expand in the radial direction mainly due to ambipolar diffusion, which is diffusion in plasma due to interaction with the electric field. Underdense meteors, which are the ones used in this study, have a plasma frequency that is lower than the frequency of the radar, which makes it possible for the radio wave from the radar to penetrate into the meteor trail and be scattered by each electron.

Echoes are detected from a region with a radius of approximately 50 km. The radar typically detects around 10 000 echoes day^{-1}, of which around 200–600 echoes are detected per hour at the peak occurrence height of 90 km. The number of echoes detected per day allows for a 30 min resolution of temperature values. The intra-day periodicity in meteor detections by the NTMR radar is less pronounced than that of lower latitude stations and we do not anticipate tidally-induced bias regarding echo rates at specific tidal phases for daily averages. The height resolution and the range resolution are both 1 km. From the decay time of the radar signal we can derive ambipolar diffusion coefficients, D_a:

$$D_a = \frac{\lambda^2}{16\pi^2\tau} \tag{1}$$

where λ is the radar wavelength and τ is the radar echo decay time. It has been shown that this coefficient also can be expressed in terms of atmospheric temperature and

ACPD
15, 15289–15317, 2015

pressure:

$$D_\mathrm{a} = 6.39 \times 10^{-2} K_0 \frac{T^2}{p} \tag{2}$$

where p is pressure, T is temperature, and K_0 is the zero-field reduced mobility factor of the ions in the trail. In this study we use the value for K_0 of $2.4 \times 10^{-4}\,\mathrm{m^2\,s^{-1}\,V^{-1}}$, in accordance with e.g. Holdsworth et al. (2006). Pressure values are derived from atmospheric densities obtained from falling sphere measurements appropriate for 70° N, combining those of Lübken and von Zahn (1991) and Lübken (1999), previously used by e.g. Holdsworth (2006) and Dyrland et al. (2010).

The NTMR radar is essentially identical to the Nippon/Norway Svalbard Meteor Radar (NSMR) located in Adventdalen on Spitsbergen at 78.33° N, 16.00° E. Further explanation of the radar and explanation of theories can be found in e.g. Hall et al. (2002, 2012), Cervera and Reid (2000) and McKinley (1961).

Calibration of temperatures derived from meteor echoes with an independent, coinciding temperature series is necessary, according to previous studies (e.g. Hocking, 1999). Temperatures from the NSMR radar have been derived most recently by Dyrland et al. (2010), employing a new calibration approach for the meteor radar temperatures, wherein temperature measurements from the Microwave Limb Sounder (MLS) on the Aura satellite were used instead of the previously used rotational hydroxyl and potassium lidar temperatures from ground-based optical instruments (Hall et al., 2006). Neither ground-based optical observations nor lidar soundings are available for the time period of interest or the location of the NTMR. In this study we therefore employ the same approach as Dyrland et al. (2010), using Aura MLS temperatures to calibrate the NTMR temperatures.

NASA's EOS Aura satellite was launched 15 July 2004 and gives daily global coverage (between 82° S and 82° N) with about 14.5 orbits per day. The MLS instrument is one of four instruments on Aura and samples viewing forward along the spacecraft's flight direction, scanning its view from the ground to ~ 90 km every ~ 25 s, making

Discussion Paper | Discussion Paper | Discussion Paper | Discussion Paper |
ACPD
15, 15289–15317, 2015
Neutral atmosphere temperature change at 90 km, 70° N, 19° E, 2003–2014
S. E. Holmen et al.

measurements of atmospheric temperature, among others (NASA Jet Propulsion Laboratory). Aura MLS temperature data (version 03) were obtained for latitude 69.7° N ± 5.0° and longitude 19.0° E ± 10.0° at pressure 0.001 hPa, corresponding to ∼ 90 km.

3 Calibration of NTMR temperatures

Figure 1 shows NTMR "raw" temperatures from November 2003 to October 2014, derived from Eqs. (1) and (2), plotted together with Aura MLS temperatures. The Aura satellite overpasses Tromsø at 01:00–03:00 and 10:00–12:00 UTC, which means that the Aura daily averages are representative for these time windows. It was therefore necessary to investigate any bias arising from Aura not measuring throughout the whole day. A way to do this is to assume that Aura temperatures and NTMR temperatures follow the same diurnal variation and thus investigate the diurnal variation of NTMR temperatures. This was done by superposing all NTMR temperatures by time of day, obtaining 48 values for each day, since the radar allows for a 30 min resolution.

There is an ongoing investigation into the possibility that D_a derived by NTMR can be affected by modified electron mobility during auroral particle precipitation. According to Rees et al. (1972), neutral temperatures in the auroral zone show a positive correlation with geomagnetic activity. It is therefore a possibility that the diurnal variation of NTMR neutral temperatures is in fact influenced by aurora, and that apparent D_a enhancements during strong auroral events do not necessarily depict neutral temperature increase. This matter requires further attention.

Investigation of possible unrealistic D_a enhancements was carried out by calculating standard errors of estimated half hourly D_a values:

$$\mathrm{se} = \frac{\sigma}{\sqrt{\mathrm{ne}}} \tag{3}$$

where σ is standard deviation and ne is the number of echoes detected by the radar. By inspection and comparison of results between one of the authors (M. Tsutsumi) and

S. Nozawa (personal communication, 2015), all half hourly D_a values with a standard error larger than 7 % of the estimated D_a value were excluded from further analysis. This rejection criterion led to that 5.4 % of the D_a values were rejected.

Figure 2 shows monthly averages of the superposed values of NTMR temperatures, after application of the D_a rejection procedure, as a function of time of day for days coinciding with Aura measurements. It is evident from the figure that the lowest temperatures are in general achieved in the forenoon, which coincides with one of the periods per day when Aura MLS makes measurements over Tromsø.

Subtracting the monthly averages of the 00:00–24:00 UTC temperatures from the 01:00–03:00 and 10:00–12:00 UTC temperatures gave the estimated biases in Aura daily means due to only sampling during some hours of the day and are given in Fig. 3. The figure shows that by judging by the measurement windows, Aura underestimates the daily mean (00:00–24:00 UTC) more during winter that during spring and summer. Note the higher standard deviations in spring and summer compared to winter.

The initially obtained Aura temperatures were corrected by adding the biases from Fig. 3 in order to arrive at daily mean temperatures that are representative for the entire day. Also, a 10 K correction for cold bias was applied to the Aura temperatures, following a suggestion from French and Mulligan (2010) from their comparison with other independent temperature measurements.

Figure 4 shows a scatterplot of the corrected Aura temperatures against the "raw" NTMR temperatures. By observing the two datasets, a seasonally dependent relationship is discernible. A 2nd degree polynomial provided the best overall fit ($R^2 = 0.87$) compared with a linear fit. The blue line represents the quadratic, least-squares fit and is described by:

$$T_{\mathrm{NTMR}} = 0.0035 T_{\mathrm{Aura}}^2 - 0.32 T_{\mathrm{Aura}} + 126 \tag{4}$$

where T_{NTMR} is the "raw" temperature obtained from NTMR, and T_{Aura} is the corrected temperature from Aura MLS. Inverting Eq. (4) enabled us to estimate NTMR temperatures calibrated with respect to Aura MLS temperatures. NTMR temperatures were

ACPD
15, 15289–15317, 2015

now corrected for the days of measurements coinciding with Aura measurements. For calibration of the remaining NTMR temperatures the same equation (Eq. 4) was used, with NTMR "raw" temperatures not coinciding with Aura measurements as input.

To estimate the calibration uncertainty, all corrected Aura temperatures were subtracted from the NTMR temperatures, and the differences were plotted in a histogram with 5 K bins. A Gaussian was fitted to the distribution. The standard deviation of the Gaussian was 8.9 K, which is then considered the overall uncertainty of the calibration. Figure 5 shows the histogram and the fitted Gaussian curve. Finally, Fig. 6 shows the calibrated NTMR temperatures with uncertainties plotted together with Aura MLS temperatures, corrected for tidal and cold bias.

4 Trend analysis

A monthly climatology of the calibrated NTMR temperatures was obtained by averaging all January, February, etc. values. The seasonal variation is shown in Fig. 7 and reveals a summer minimum of around 150–160 K and a winter maximum of around 200–210 K. The monthly values were then subtracted from the daily calibrated temperatures, obtaining daily residuals independent of seasonal variation.

There are several measures of solar variability available, e.g. the F10.7 cm solar radio flux, the sunspot number (SSN), total solar irradiance (TSI), Mg II 280 nm core-to-wing ratio UV-index and the flare index (FI). These indices are considered proxies for solar radiation formed on different altitudes of the solar atmosphere and are highly correlated (Bruevich et al., 2014). In this study we use the F10.7 cm flux as a proxy for solar activity, which is the most commonly used index in middle/upper atmospheric temperature trend studies (e.g. Laštovička et al., 2008; Hall et al., 2012).

A 30 day running mean filter was applied to the daily residual temperatures. Figure 8 shows the residuals plotted against corresponding F10.7 cm values. The straight, red line in the figure gave the best linear fit to the daily residuals with a 30 day running mean applied and gave a solar response coefficient of $4.2\,\mathrm{K} \pm 0.3\,\mathrm{K}\,(100\,\mathrm{SFU})^{-1}$ (1 SFU = 1 solar flux unit = $10^{-22}\,\mathrm{W\,m^{-2}\,Hz^{-1}}$).

From Fig. 8 there appears to be a somewhat non-linear relationship between the temperatures at 90 km height and the F10.7 cm index. There seems to be a tendency of a less steep increase in temperatures toward higher F10.7 values. Ogawa et al. (2014) also found a non-linear relationship between upper atmospheric temperatures and solar activity using EISCAT UHF radar observations from Tromsø, even though it must be noted that the altitude range they looked at differs from ours. In Fig. 8 we have therefore also plotted the quadratic, least-squares fit to the running mean values. Lacking any objective scientific basis to do otherwise, we chose to fit a 2nd degree polynomial following the philosophy of Ogawa et al. (2014), although it is conceivable that other functions could be more suitable. The 2nd degree polynomial gave us a better fit to the residuals ($R^2 = 0.17$) compared to the straight line ($R^2 = 0.07$). We subtracted the solar response from the dataset of daily, seasonally corrected residuals using this relation:

$$T' = T - (a \cdot f10.7^2 + b \cdot f10.7 + c) \tag{5}$$

where T' is the new set of residual temperatures with seasonal and solar response subtracted, T is the residual temperatures with only seasonal variation subtracted, $f10.7$ is the daily F10.7 cm flux corresponding to T, and a, b and c are coefficients of the 2nd degree polynomial ($a = -0.0015$, $b = 0.37$, $c = -21$).

From the new set of temperature residuals we calculated monthly means. This was done to remove any high-frequency deterministic component, such as that resulting from multi-day period waves. Finally, the linear trend was found by performing linear regression using a least-squares fit. The long-term linear temperature trend using monthly means is $-3.6\,\mathrm{K} \pm 1.1\,\mathrm{K\,decade^{-1}}$. This trend can be considered statistically significant (i.e. significantly non-zero at the 5 % level), since the uncertainty ($2\sigma = 2.2\,\mathrm{K\,decade^{-1}}$) is less than the trend itself (Tiao et al., 1990). Figure 9 shows the linear trend of the monthly values for the whole dataset, from November 2003 through

ACPD
15, 15289–15317, 2015

October 2014. For comparison, the long-term trend using daily temperature values is $-3.4\,\mathrm{K} \pm 0.5\,\mathrm{K\,decade^{-1}}$.

In addition to the average temperature change, we also treated summer and winter seasons separately. First, trends for each month were investigated using the same approach as for the average regardless of month. Figure 10 shows the result. Then, averages of November, December and January, and of May, June and July were made. They were defined as "winter" and "summer", respectively. The long-term linear winter trend is $-8.1\,\mathrm{K} \pm 2.5\,\mathrm{K\,decade^{-1}}$, and the long-term summer trend is $-0.8\,\mathrm{K} \pm 2.9\,\mathrm{K\,decade^{-1}}$.

The trend analysis was also performed without carrying out the D_a rejection procedure explained in Sect. 3. Final results with and without data rejection do not differ significantly considering the calculated uncertainties.

5 Discussion

5.1 Suitability of a meteor radar for estimation of neutral temperatures at 90 km height

As explained in Sect. 2, neutral air temperatures derived from meteor trail echoes depend on pressure, p, the zero-field reduced mobility of the ions in the trail, K_0, and ambipolar diffusion coefficients, D_a. K_0 will depend on the ion composition in the meteor trail, as well as the chemical composition of the atmosphere. The chemical composition of the atmosphere is assumed to not change significantly with season (Hocking, 2004). Unfortunately, the exact content of a meteor trail is unknown. Usually, a value for K_0 between 1.9×10^{-4} and $2.9 \times 10^{-4}\,\mathrm{m^2\,s^{-1}\,V^{-1}}$ is chosen, depending on what ion one assumes to be the main ion of the trail (Hocking et al., 1997). Even though we in this study have chosen a constant value for K_0 of $2.4 \times 10^{-4}\,\mathrm{m^2\,s^{-1}\,V^{-1}}$, some variability in K_0 is expected. According to Hocking (2004) variability can occur due to fragmentation of the incoming meteoroid, anisotropy in the diffusion rate, plasma instabilities and vari-

ACPD
15, 15289–15317, 2015

ations in the composition of the meteor trail. Using computer simulations, they reported a typical variability in K_0 from meteor to meteor of 27 % and that the variability is most dominant at higher temperatures. Based on this, we cannot rule out sources of error due to the choice of K_0 as a constant, but since we have no possibility to analyse the composition of all meteor trails detected by the radar we have no other choice than to choose a constant value for K_0.

How well ambipolar diffusion coefficients obtained for 90 km altitude are suited for calculating neutral temperatures has previously been widely discussed, e.g. by Hall et al. (2012) for the trend analysis of the Svalbard meteor radar data, but will be shortly repeated here. For calculations of temperatures using meteor radar, ambipolar diffusion alone is assumed to determine the decay of the underdense echoes. Diffusivities are expected to increase exponentially with height through the region from which meteor echoes are obtained (Ballinger et al., 2008; Chilson et al., 1996). Hall et al. (2005) found that this is only the case between ~ 85 and ~ 95 km altitude, using diffusion coefficients delivered by NTMR from 2004. They found diffusivities less than expected above ~ 95 km and diffusivities higher than expected below ~ 85 km. Ballinger et al. (2008) got a similar result using meteor observations over northern Sweden. It has been proposed that processes other than ambipolar diffusion influence meteor decay times. If this is the case it may have consequences for the estimation of temperatures, and therefore it is important to investigate this further.

Departures of the anticipated exponential increase with height of molecular diffusion above ~ 95 km have in previous studies been attributed to gradient-drift Farley–Buneman instability. Farley–Buneman instability occurs where the trail density gradient and electric field are largest. Due to frequent collisions with neutral particles, electrons are magnetised while ions are left unmagnetised, causing electrons and ions to differ in velocity. Electrons then create an electric field perpendicular to the meteor trail, leading to anomalous fading times that can be an order of magnitude higher than those expected from ambipolar diffusion. The minimum altitude at which this occurs depends on the trail altitude, density gradient and latitude, and at high latitudes this altitude is

ACPD
15, 15289–15317, 2015

~ 95 km. Therefore, using ambipolar diffusion rates to calculate trail altitudes above this minimum altitude may lead to errors of several kilometres, due to that the diffusion coefficients derived from the measurements are underestimated (Ballinger et al., 2008; Dyrud et al., 2001; Kovalev et al., 2008).

Reasons for the higher diffusivities than expected according to theory below ~ 85 km are not completely understood. Hall (2002) proposed that neutral turbulence may be responsible for overestimates of molecular diffusivity in the region ~ 70–85 km, but this hypothesis was rejected by Hall et al. (2005) due to a lacking correlation between neutral air turbulent intensity and diffusion coefficients delivered by the NTMR radar. Other mechanisms for overestimates of molecular diffusivity include incorrect determination of echo altitude and fading times due to limitations of the radar (Hall et al., 2005).

Since the peak echo occurrence height is 90 km and this is also the height at which a minimum of disturbing effects occur, 90 km height is therefore considered the optimal height for temperature measurements using meteor radar. Ballinger et al. (2008) report that meteor radars in general deliver reliable daily temperature estimates near the mesopause using the method outlined in this study, but emphasize that one should exercise caution when assuming that observed meteor echo fading times are primarily governed by ambipolar diffusion. They proposed, after Havnes and Sigernes (2005), that electron-ion recombination can impact meteor echo decay times. Especially can this affect the weaker echoes, and hence can this effect lead to underestimation of temperatures.

Determination of temperatures from meteor radar echo times is a non-trivial task, mainly because the calculation of ambipolar diffusion coefficients depends on the ambient atmospheric pressure. By using radar echo decay times to calculate ambipolar diffusion coefficients from Eq. (1), we can from Eq. (2) get an estimate for T^2/p. Input of pressure values into the equation will thus provide atmospheric temperatures. However, measurements of pressure are rare and difficult to achieve at 90 km height, and often one has to rely on model values. Traditionally, pressure values at 90 km have been calculated using the ideal gas law, taking total mass density from atmospheric models,

Discussion Paper | Discussion Paper | Discussion Paper | Discussion Paper |

ACPD

15, 15289–15317, 2015

Neutral atmosphere temperature change at 90 km, 70° N, 19° E, 2003–2014

S. E. Holmen et al.

e.g. the MSISE models, where the newest version is NRLMSIS-00. It is hard to verify the pressure values derived from the models because of lack of measurements to compare the model to, and hence using the pressure values may result in uncertainties of estimated atmospheric temperatures. In this study, we obtained pressure values from measurements of mass densities obtained from falling spheres combined with sodium lidar from Andøya (69° N, 15.5° E) (Lübken, 1999; Lübken and von Zahn, 1991). All measurements have been combined to give a yearly climatology, that is, one pressure value for each day of the year. Since Andøya is located in close proximity to Tromsø (approximately 120 km), the pressure values are considered appropriate for our calculations of neutral temperatures. One disadvantage with using pressure values obtained from the falling sphere measurements is that no day-to-day variations are taken into account, only the average climatology.

5.2 Physical explanations for cooling and comparison with other studies

Other studies on long-term mesospheric temperature trends from mid and high latitudes yield mostly negative or near-zero trends. Few studies cover the same time period as ours, and few are from locations close to Tromsø. Hall et al. (2012) reported a negative trend of $-4\,\mathrm{K} \pm 2\,\mathrm{K\,decade}^{-1}$ for temperatures derived from the meteor radar from Longyearbyen, Svalbard (78° N, 16° E) at 90 km height over the time period 2001 to 2011, while Holmen et al. (2014) found a near-zero trend for OH^* airglow temperatures at ~ 87 km height over Longyearbyen over the longer time period 1983 to 2013. Offermann et al. (2010) reported a trend of $-2.3\,\mathrm{K} \pm 0.6\,\mathrm{K\,decade}^{-1}$ for ~ 87 km height using OH^* airglow measurements from Wuppertal (51° N, 7° E). It must be noted that the peak altitude of the OH^* airglow layer can range from 75 to > 90 km (Winick et al., 2009) and thus affect the comparability of OH^* airglow temperature trends and meteor radar temperature trends. Beig (2011) reported that most recent studies on mesopause region temperature trends show weak negative trends, which is in line with our results.

Our results indicate a cooling at 90 km altitude over Tromsø. A general cooling of the middle atmosphere will cause a contraction of the atmospheric column and hence a lowering of upper mesospheric pressure surfaces. The pressure model used as input to Eq. (2) is only seasonally dependent, so a possible trend in pressure at 90 km must be addressed. By looking at Eq. (2), it is evident that if pressure decreases, temperature will decrease even more. By incorporating a decreasing trend in the pressure model will then serve to further strengthen the negative temperature trend we observe.

It has been proposed that GWs may be a major cause of negative temperature trends in the mesosphere and thermosphere (Beig, 2011; Oliver et al., 2013). GWs effectively transport chemical species and heat in the region, and increased GW drag leads to cooling. However, there are large regional differences regarding trends in GW activity. Hoffmann et al. (2011) found an increasing GW activity in the mesosphere in summer for selected locations, but Jacobi (2014) found larger GW amplitudes during solar maximum and related this to a stronger mesospheric jet during solar maximum, both for winter and summer. Since we have not conducted any gravity wave trend assessment in this study, we cannot conclude that GW activity is responsible for the negative temperature trend, but we cannot rule out its role either.

The stronger cooling trend for winter compared to summer is consistent with model studies. Schmidt et al. (2006) and Fomichev et al. (2007) show, using the HAMMONIA and CMAM models, respectively, that a doubling of the CO_2 concentration will lead to a general cooling of the middle atmosphere, but that the high-latitude summer mesopause will experience insignificant change or even slight warming. They propose that this is the result of both radiative and dynamical effects. In summer, the CO_2 radiative forcing is positive due to heat exchange between the cold polar mesopause and the warmer, underlying layers. Also, CO_2 doubling alters the mesospheric residual circulation. This change is caused by a warming in the tropical troposphere and cooling in the extratropical tropopause, leading to a stronger equator-to-pole temperature gradient and hence stronger midlatitude tropospheric westerlies. This causes the westerly gravity wave drag to weaken, resulting in decreased adiabatic cooling from a slower ascent of the upper mesospheric circulation.

6 Conclusions

The long-term trend of neutral temperatures at 90 km height derived from the NTMR radar in Ramfjordmoen, Tromsø, with seasonality and solar response subtracted, is $-3.6\,\mathrm{K} \pm 1.1\,\mathrm{K\,decade}^{-1}$. The linear fit between the smoothed daily residuals and corresponding F10.7 cm values gave a solar response coefficient of $4.2\,\mathrm{K} \pm 0.3\,\mathrm{K}\,(100\,\mathrm{SFU})^{-1}$. However, a 2nd degree polynomial gave the best fit to the data and was thus used for correcting the dataset of solar response. When looking at summer and winter seasons separately, the trends are $-0.8\,\mathrm{K} \pm 2.9\,\mathrm{K\,decade}^{-1}$ for summer and $-8.1\,\mathrm{K} \pm 2.5\,\mathrm{K\,decade}^{-1}$ for winter.

Final results of the trend analysis, both when excluding and including rejection of D_a values due to hypothetical anomalous electrodynamic processes, do not differ significantly. It is reasonable to believe that strong geomagnetic conditions can affect derived temperatures on a short time scale. However, due to the considerable quantity of data employed in this study, it is inconceivable that this effect will change the conclusions regarding trends, as our results also show.

90 km is considered the optimal height for retrieval of neutral temperatures using ambipolar diffusion coefficients from NTMR, due to that the peak echo occurrence height detected by the radar is 90 km and that this is also the height at which a minimum of disturbing effects occur. Above ~ 95 km anomalous fading times that can be an order of magnitude higher than those expected from ambipolar diffusion may be measured, due to gradient-drift Farley–Buneman instability, causing the derived ambipolar diffusion to be underestimated. Below ~ 85 km higher diffusivities than expected according to theory in which the temperature estimation is based on may be encountered, due to reasons not fully understood.

A weak cooling trend is in line with other recent studies on mesopause region temperature trends. A cooling of the middle atmosphere will cause a lowering of upper mesospheric pressure surfaces. By implementing a negative trend in pressure at 90 km into the equation we use for estimating temperatures the negative temperature trend is

ACPD
15, 15289–15317, 2015

enhanced, which reinforces our finding of a cooling trend. The most accepted theory behind a cooling of the middle atmosphere is increased greenhouse gas emissions, but also dynamics may play a significant role. Our results yield a more negative trend in winter compared to summer, which may be explained by both radiative and dynamical effects. In summer, a larger heat exchange takes place from atmospheric layers below the cold, polar mesopause. Weakening of gravity wave drag leads to weakening of the mesospheric residual circulation, which counteracts cooling. These effects occur due to increased CO_2 concentrations in the atmosphere, according to model studies.

Acknowledgements. The research for this article was financially supported by The Research Council of Norway through contract 223252/F50 (CoE). NTMR operation was supported by Research Project KP-0 of National Institute of Polar Research. The authors wish to thank Frank Mulligan at Maynooth University, Ireland, for providing the NASA EOS Aura MLS temperatures.

References

Akmaev, R. A. and Fomichev, V. I.: Cooling of the mesosphere and lower thermosphere due to doubling of CO_2, Ann. Geophys., 16, 1501–1512, doi:10.1007/s00585-998-1501-z, 1998.

Akmaev, R. A. and Fomichev, V. I.: A model estimate of cooling in the mesosphere and lower thermosphere due to the CO_2 increase over the last 3–4 decades, Geophys. Res. Lett., 27, 2113–2116, doi:10.1029/1999GL011333, 2000.

Ballinger, A. P., Chilson, P. B., Palmer, R. D., and Mitchell, N. J.: On the validity of the ambipolar diffusion assumption in the polar mesopause region, Ann. Geophys., 26, 3439–3443, doi:10.5194/angeo-26-3439-2008, 2008.

Beig, G.: Long-term trends in the temperature of the mesosphere/lower thermosphere region: 1. Anthropogenic influences, J. Geophys. Res.-Space, 116, A00H11, doi:10.1029/2011JA016646, 2011.

Bruevich, E. A., Bruevich, V. V., and Yakunina, G. V.: Changed relation between solar 10.7-cm radio flux and some activity indices which describe the radiation at different altitudes of atmosphere during cycles 21–23, J. Astrophys. Astron., 35, 1–15, 2014.

Cervera, M. A. and Reid, I. M.: Comparison of atmospheric parameters derived from meteor observations with CIRA, Radio Sci., 35, 833–843, doi:10.1029/1999RS002226, 2000.
Chilson, P. B., Czechowsky, P., and Schmidt, G.: A comparison of ambipolar diffusion coefficients in meteor trains using VHF radar and UV lidar, Geophys. Res. Lett., 23, 2745–2748, doi:10.1029/96gl02577, 1996.
Dyrland, M. E., Hall, C. M., Mulligan, F. J., Tsutsumi, M., and Sigernes, F.: Improved estimates for neutral air temperatures at 90 km and 78° N using satellite and meteor radar data, Radio Sci., 45, RS4006, doi:10.1029/2009rs004344, 2010.
Dyrud, L. P., Oppenheim, M. M., and vom Endt, A. F.: The anomalous diffusion of meteor trails, Geophys. Res. Lett., 28, 2775–2778, 2001.
Fomichev, V. I., Jonsson, A. I., de Grandpré, J., Beagley, S. R., McLandress, C., Semeniuk, K., and Shepherd, T. G.: Response of the middle atmosphere to CO_2 doubling: results from the Canadian Middle Atmosphere Model, J. Climate, 20, 1121–1144, doi:10.1175/JCLI4030.1, 2007.
French, W. J. R. and Mulligan, F. J.: Stability of temperatures from TIMED/SABER v1.07 (2002–2009) and Aura/MLS v2.2 (2004–2009) compared with OH(6-2) temperatures observed at Davis Station, Antarctica, Atmos. Chem. Phys., 10, 11439–11446, doi:10.5194/acp-10-11439-2010, 2010.
Hall, C. M.: On the influence of neutral turbulence on ambipolar diffusivities deduced from meteor trail expansion, Ann. Geophys., 20, 1857–1862, doi:10.5194/angeo-20-1857-2002, 2002.
Hall, C. M., Aso, T., Tsutsumi, M., Nozawa, S., Manson, A. H., and Meek, C. E.: *Letter to the Editior* Testing the hypothesis of the influence of neutral turbulence on the deduction of ambipolar diffusivities from meteor trail expansion, Ann. Geophys., 23, 1071–1073, doi:10.5194/angeo-23-1071-2005, 2005.
Hall, C. M., Aso, T., Tsutsumi, M., Höffner, J., Sigernes, F., and Holdsworth, D. A.: Neutral air temperatures at 90 km and 70° N and 78° N, J. Geophys. Res., 11, D14105, doi:10.1029/2005JD006794, 2006.
Hall, C. M., Dyrland, M. E., Tsutsumi, M., and Mulligan, F. J.: Temperature trends at 90 km over Svalbard, Norway (78° N 16° E), seen in one decade of meteor radar observations, J. Geophys. Res.-Atmos., 117, D08104, doi:10.1029/2011JD017028, 2012.
Havnes, O. and Sigernes, F.: On the influence of background dust on radar scattering from meteor trails, J. Atmos. Sol.-Terr. Phy., 67, 659–664, doi:10.1016/j.jastp.2004.12.009, 2005.

ACPD
15, 15289–15317, 2015

Neutral atmosphere temperature change at 90 km, 70° N, 19° E, 2003–2014

S. E. Holmen et al.

Hocking, W. K.: Temperatures using radar-meteor decay times, Geophys. Res. Lett., 26, 3297–3300, doi:10.1029/1999GL003618, 1999.
Hocking, W. K.: Radar meteor decay rate variability and atmospheric consequences, Ann. Geophys., 22, 3805–3814, doi:10.5194/angeo-22-3805-2004, 2004.
Hocking, W. K., Thayaparan, T., and Jones, J.: Meteor decay times and their use in determining a diagnostic mesospheric temperature-pressure parameter: methodology and one year of data, Geophys. Res. Lett., 24, 2977–2980, doi:10.1029/97gl03048, 1997.
Hoffmann, P., Rapp, M., Singer, W., and Keuer, D.: Trends of mesospheric gravity waves at northern middle latitudes during summer, J. Geophys. Res., 116, D00P08, doi:10.1029/2011JD015717, 2011.
Holdsworth, D. A., Morris, R. J., Murphy, D. J., Reid, I. M., Burns, G. B., and French, W. J. R.: Antarctic mesospheric temperature estimation using the Davis mesosphere–stratosphere–troposphere radar, J. Geophys. Res.-Atmos., 111, D05108, doi:10.1029/2005jd006589, 2006.
Holmen, S. E., Dyrland, M. E., and Sigernes, F.: Long-term trends and the effect of solar cycle variations on mesospheric winter temperatures over Longyearbyen, Svalbard (78° N), J. Geophys. Res.-Atmos., 119, 6596–6608, doi:10.1002/2013jd021195, 2014.
Jacobi, C.: Long-term trends and decadal variability of upper mesosphere/lower thermosphere gravity waves at midlatitudes, J. Atmos. Sol.-Terr. Phy., 118, 90–95, doi:10.1016/j.jastp.2013.05.009, 2014.
Kovalev, D. V., Smirnov, A. P., and Dimant, Y. S.: Modeling of the Farley-Buneman instability in the E-region ionosphere: a new hybrid approach, Ann. Geophys., 26, 2853–2870, doi:10.5194/angeo-26-2853-2008, 2008.
Laštovička, J., Akmaev, R. A., Beig, G., Bremer, J., Emmert, J. T., Jacobi, C., Jarvis, M. J., Nedoluha, G., Portnyagin, Yu. I., and Ulich, T.: Emerging pattern of global change in the upper atmosphere and ionosphere, Ann. Geophys., 26, 1255–1268, doi:10.5194/angeo-26-1255-2008, 2008.
Laštovička, J., Solomon, S. C., and Qian, L.: Trends in the neutral and ionized upper atmosphere, Space Sci. Rev., 168, 113–145, doi:10.1007/s11214-011-9799-3, 2012.
Lübken, F.-J.: Thermal structure of the Arctic summer mesosphere, J. Geophys. Res.-Atmos., 104, 9135–9149, 1999.
Lübken, F.-J. and von Zahn, U.: Thermal structure of the mesopause region at polar latitudes, J. Geophys. Res.-Atmos., 96, 20841–20857, doi:10.1029/91JD02018, 1991.

ACPD
15, 15289–15317, 2015

Manabe, S. and Wetherald, R. T.: The effects of doubling the CO_2 concentration on the climate of a general circulation model, J. Atmos. Sci., 32, 3–15, 1975.
McKinley, D. W. R.: Meteor Science and Engineering, McGraw-Hill, New York, 1961.
NASA Jet Propulsion Laboratory: EOS Microwave Limb Sounder, available at: http://mls.jpl.nasa.gov/index-eos-mls.php, last access: January 2015.
Offermann, D., Hoffmann, P., Knieling, P., Koppmann, R., Oberheide, J., and Steinbrecht, W.: Long-term trends and solar cycle variations of mesospheric temperatures and dynamics, J. Geophys. Res., 115, D18127, doi:10.1029/2009JD013363, 2010.
Ogawa, Y., Motoba, T., Buchert, S. C., Häggström, I., and Nozawa, S.: Upper atmosphere cooling over the past 33 years, Geophys. Res. Lett., 41, 5629–5635, doi:10.1002/2014GL060591, 2014.
Oliver, W. L., Zhang, S.-R., and Goncharenko, L. P.: Is thermospheric global cooling caused by gravity waves?, J. Geophys. Res.-Space, 118, 3898–3908, doi:10.1002/jgra.50370, 2013.
Rees, D., Rishbeth, H., and Kaiser, T. R.: Winds and temperatures in the auroral zone and their relations to geomagnetic activity, Philos. T. R. Soc. S.-A, 271, 563–575, 1972.
Roble, R. G. and Dickinson, R. E.: How will changes in carbon dioxide and methane modify the mean structure of the mesosphere and thermosphere?, Geophys. Res. Lett., 16, 1441–1444, 1989.
Schmidt, H., Brasseur, G. P., Charron, M., Manzini, E., Giorgetta, M. A., and Diehl, T.: The HAMMONIA Chemistry Climate Model: sensitivity of the mesopause region to the 11-year solar cycle and CO_2 doubling, J. Climate, 19, 3903–3931, doi:10.1175/JCLI3829.1, 2006.
Tiao, G. C., Reinsel, G. C., Xu, D., Pedrick, J. H., Zhu, X., Miller, A. J., DeLuisi, J. J., Mateer, C. L., and Wuebbles, D. J.: Effects of autocorrelation and temporal sampling schemes on estimates of trend and spatial correlation, J. Geophys. Res.-Atmos., 95, 20507–20517, doi:10.1029/JD095iD12p20507, 1990.
Winick, J. R., Wintersteiner, P. P., Picard, R. H., Esplin, D., Mlynczak, M. G., Russell III, J. M., and Gordley, L. L.: OH layer characteristics during unusual boreal winters of 2004 and 2006, J. Geophys. Res., 114, A02303, doi:10.1029/2008JA013688, 2009.

ACPD
15, 15289–15317, 2015

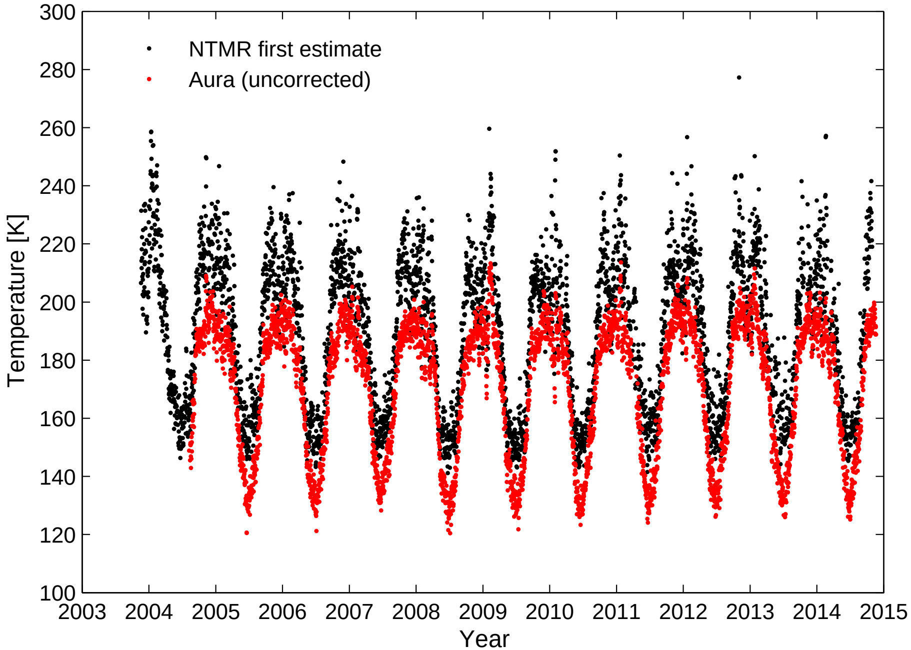

Figure 1. NTMR "raw" temperatures derived from Eqs. (1) and (2), plotted together with Aura MLS temperatures.

ACPD
15, 15289–15317, 2015

Neutral atmosphere temperature change at 90 km, 70° N, 19° E, 2003–2014

S. E. Holmen et al.

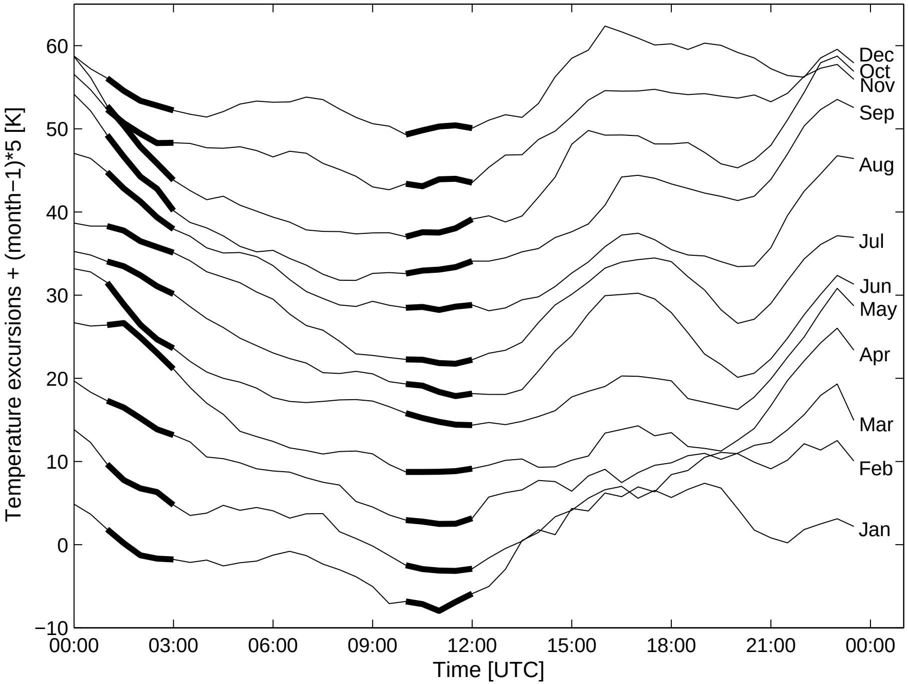

Figure 2. Monthly averages of diurnal temperature variation derived from NTMR at 90 km altitude. For clarity time series are displaced by 5 K month^{-1} subsequent to January. The time of day corresponding to when Aura makes measurements over Tromsø (01:00–03:00 and 10:00–12:00 UTC) is highlighted.

ACPD
15, 15289–15317, 2015

Neutral atmosphere temperature change at 90 km, 70° N, 19° E, 2003–2014

S. E. Holmen et al.

Title Page
Abstract | Introduction
Conclusions | References
Tables | Figures
◂ ▸
Back | Close
Full Screen / Esc
Printer-friendly Version
Interactive Discussion

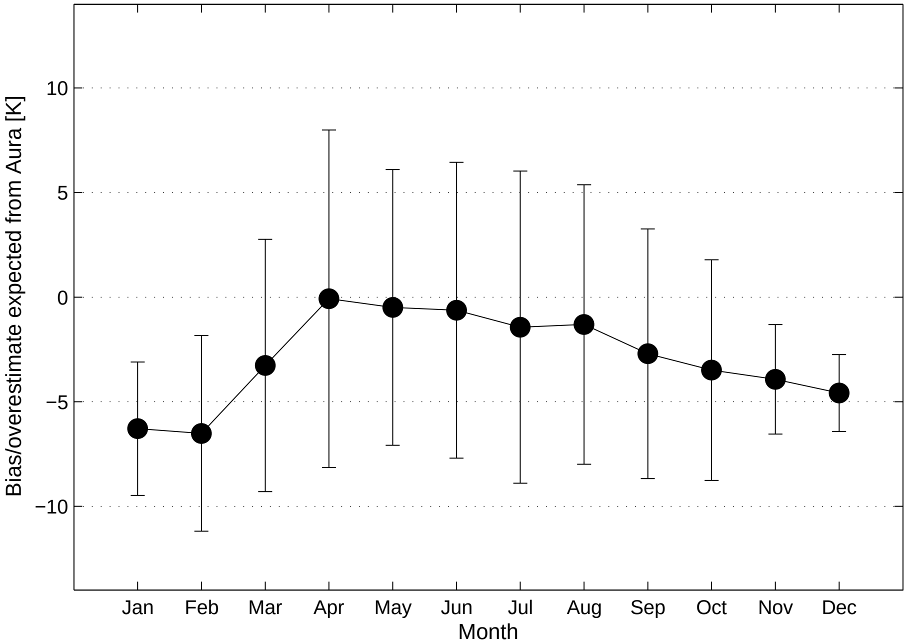

Figure 3. Bias in Aura monthly averages due to that Aura MLS only measures between 01:00 and 03:00 UTC, and between 10:00 and 12:00 UTC. Error bars represent standard deviations.

ACPD
15, 15289–15317, 2015

Neutral atmosphere temperature change at 90 km, 70° N, 19° E, 2003–2014

S. E. Holmen et al.

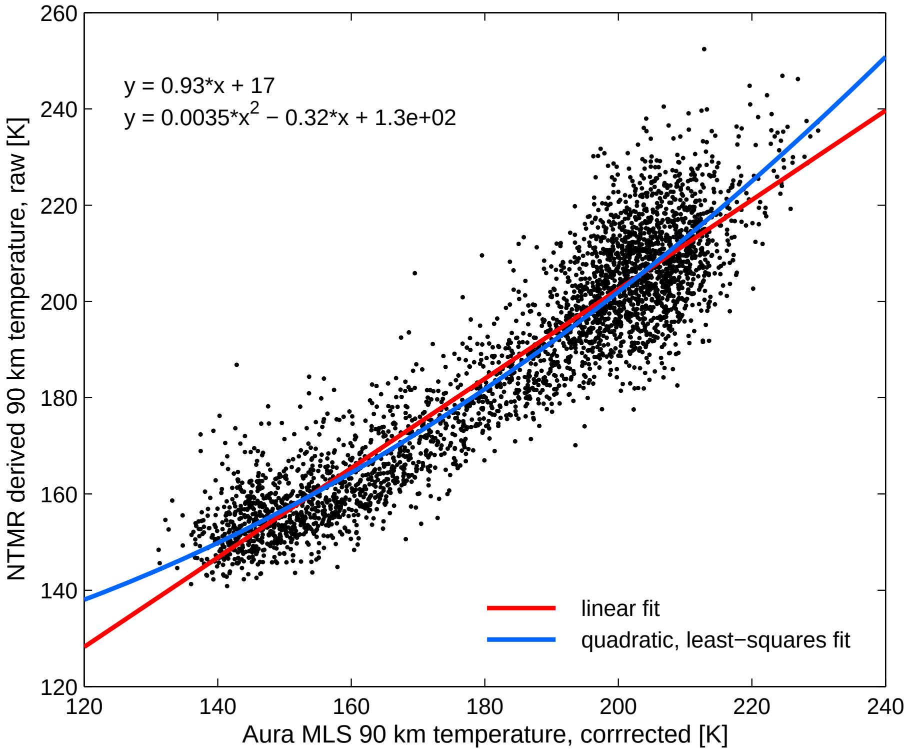

Figure 4. Scatterplot of Aura temperatures corrected for cold and time-of-day measurement bias against NTMR "raw" temperatures. The blue line represents the quadratic least-squares fit, which is the approach used in the further calibration of the NTMR temperatures. The red line represents the linear fit and is only shown for comparison.

ACPD
15, 15289–15317, 2015

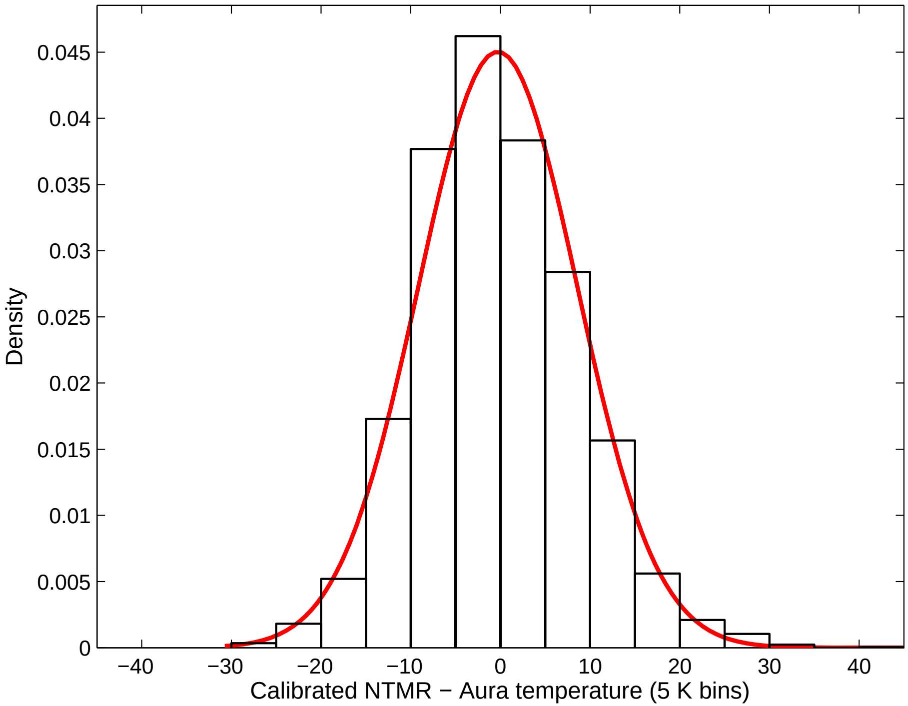

Figure 5. Histogram of the differences between calibrated NTMR temperatures and corrected Aura MLS temperatures. The red curve is a fitted Gaussian to the distribution.

ACPD
15, 15289–15317, 2015

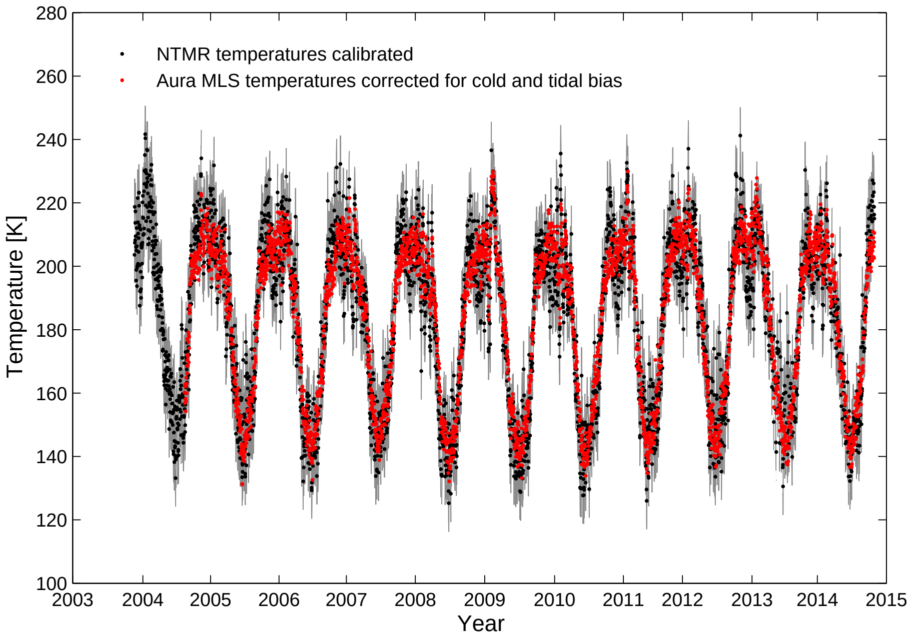

Figure 6. Calibrated NTMR temperatures plotted together with Aura MLS temperatures, corrected for tidal and cold bias. The overall calibration uncertainty is indicated by the grey shading.

ACPD
15, 15289–15317, 2015

Neutral atmosphere temperature change at 90 km, 70° N, 19° E, 2003–2014

S. E. Holmen et al.

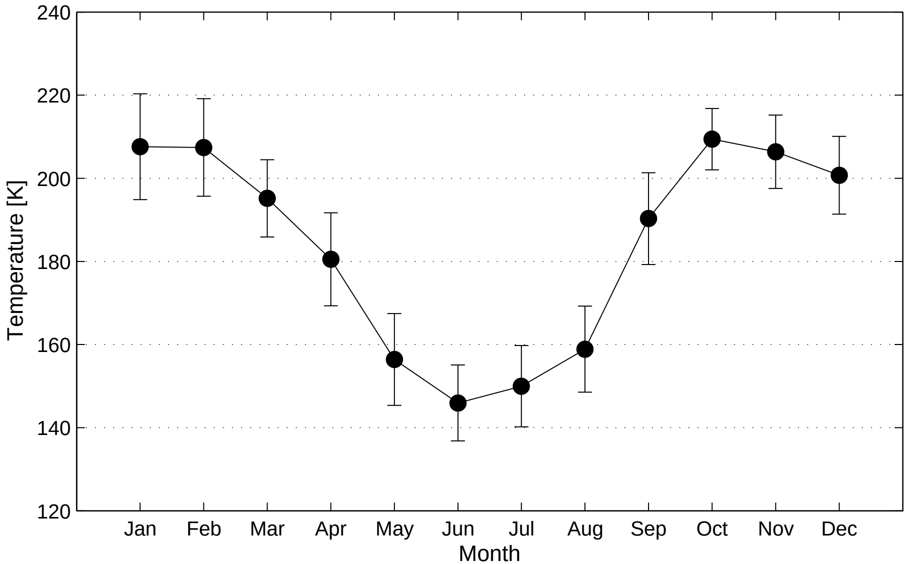

Figure 7. Monthly climatology of the NTMR temperatures obtained for 90 km altitude, using calibrated temperatures from November 2003 through October 2014. Standard deviations are shown as error bars.

ACPD
15, 15289–15317, 2015

Neutral atmosphere temperature change at 90 km, 70° N, 19° E, 2003–2014

S. E. Holmen et al.

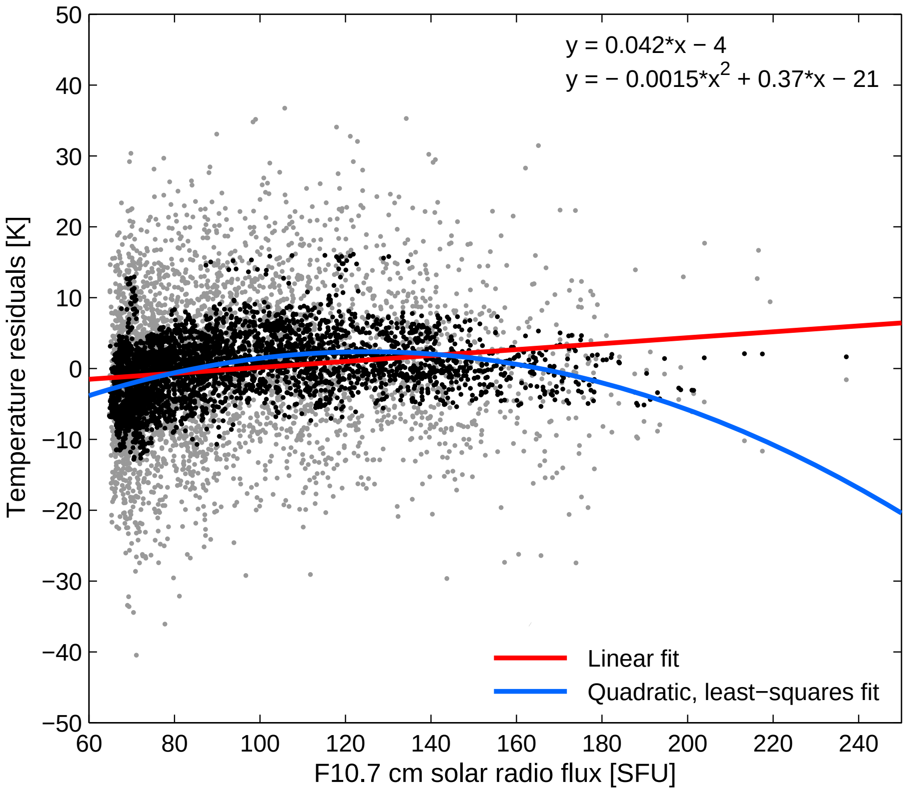

Figure 8. Scatterplot of daily averaged residuals against the corresponding F10.7 cm solar flux values. Grey dots are daily residuals, while black dots are the residuals with a 30 day running mean applied. The red line is the linear fit to the daily residuals with the 30 day running mean applied, while the blue line is the quadratic, least-squares fit.

ACPD
15, 15289–15317, 2015

Neutral atmosphere temperature change at 90 km, 70° N, 19° E, 2003–2014

S. E. Holmen et al.

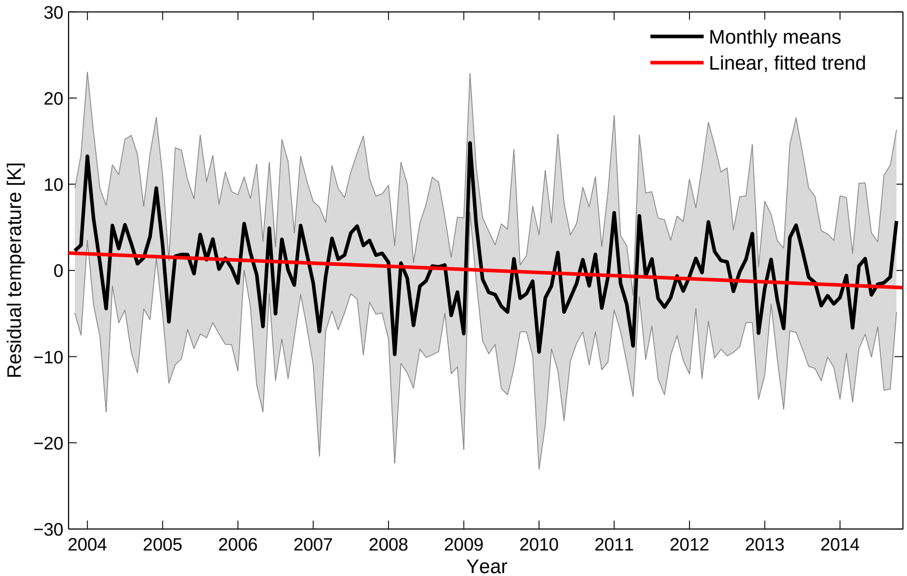

Figure 9. Monthly means of NTMR residual temperatures, corrected for climatology and solar response. The grey shading yields standard deviations.

ACPD
15, 15289–15317, 2015

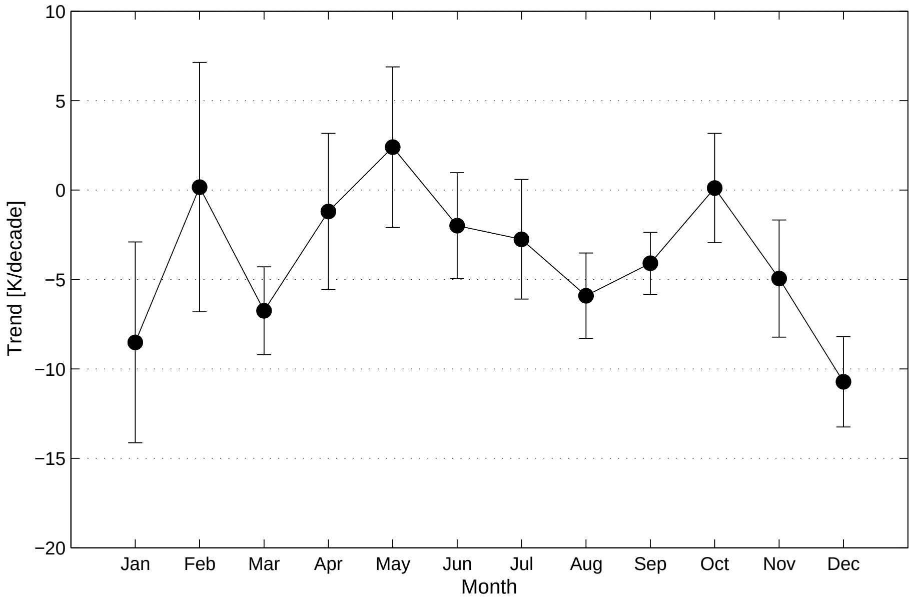

Figure 10. Monthly long-term temperature trends at 90 km altitude over Tromsø. Standard deviations are given as error bars.

ACPD
15, 15289–15317, 2015

Neutral atmosphere temperature change at 90 km, 70° N, 19° E, 2003–2014

S. E. Holmen et al.

Title Page
Abstract | Introduction
Conclusions | References
Tables | Figures
◀ | ▶
◀ | ▶
Back | Close
Full Screen / Esc
Printer-friendly Version
Interactive Discussion